ChemComm

COMMUNICATION

View Article Online
View Journal | View Issue

Cite this: *Chem. Commun.*, 2014, **50**, 4200

Received 29th December 2013,
Accepted 13th February 2014

DOI: 10.1039/c3cc49825e

www.rsc.org/chemcomm

Unprecedented catalytic performance in disordered nickel niobate through photo-synergistic promotion†

Yiguo Su, Xin Xin, Yafang Wang, Tingting Wang and Xiaojing Wang*

A novel catalyst was successfully prepared, which shows superior catalytic activity and stability toward reduction of 4-nitrophenol due to a unique photo-synergistic catalytic mechanism that relies on a synergy between thermal active sites and photogenerated electrons in $NiNb_2O_6$ nanoparticles.

Chemical transformations *via* a catalytic reduction/oxidation process at nanoparticle (NP) surfaces have drawn much attention for their applications in diverse fields.[1] Particularly, the efficient transformation of substituted nitrobenzenes to the corresponding anilines is of great importance because nitrobenzenes are generally generated as by-products and are toxic to the environment, whereas aminobenzenes are highly valuable and important components in many industrial chemicals.[2] Numerous investigations have been devoted to constructing free or immobilized NPs for the efficient reduction of nitrobenzenes.[3] However, the majority of investigations have focused merely on metallic NPs, especially noble metal NPs. In view of novel commercial opportunities, it is highly necessary to explore novel and highly active catalysts and comprehend the underling physics and chemistry that meets the green chemistry principles.

Metal niobates is a very important family of inorganic materials that has high potential applications in various fields.[4] As a typical metal niobate, $NiNb_2O_6$ represents a prototype *Columbite* structure with a close structural link to many materials. Therefore, an experimental identification of the nanoscale structure and electronic properties of $NiNb_2O_6$ is advantageous for tuning its catalytic performances as well as other *Columbite*-type NPs. Herein, highly disordered $NiNb_2O_6$ NPs were taken as model compounds for the reduction of 4-nitrophenol (4-NP) to 4-aminophenol (4-AP) based on the following considerations: (1) cheap Ni-based transition metal NPs are attractive and effective catalysts for direct catalytic reduction of nitrobenzenes.[5] (2) The chemical activity of NPs is closely related to defect chemistry. For instance, highly defective TaO_xN_y NPs exhibited outstanding activity toward catalytic reduction of nitrobenzenes.[6] (3) Photocatalytic reduction of nitrobenzenes can be achieved in the presence of hole scavengers.[7] Consequently, the synergistic utilization of a defective solid, photogenerated electrons and a suitable reductant to promote this transformation may be an effective strategy for the design of novel catalysts.

Disordered $NiNb_2O_6$ NPs with a BET surface area of 46.5 $m^2\ g^{-1}$ were successfully prepared (ESI-1†). Fig. 1a shows the XRD pattern of $NiNb_2O_6$ NPs. All diffraction peaks can be indexed to a *Columbite* phase of $NiNb_2O_6$, while no traces of impurity peaks of Nb_2O_5 and NiO were observed. It should be noted that the diffraction peaks at about 24.38° and 30.49° were significantly broadened. Due to

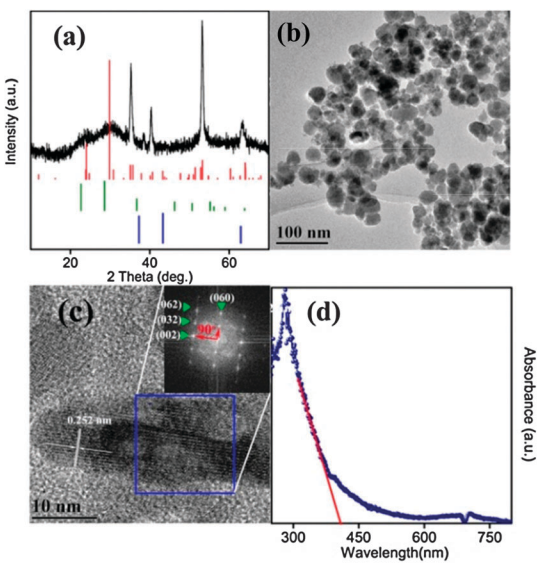

Fig. 1 XRD pattern (a), TEM image (b), HRTEM image (c) and UV-vis diffuse reflectance spectrum (d) of $NiNb_2O_6$ NPs. Vertical bars in (a) represent the standard diffraction data for $NiNb_2O_6$ (JCPDS No. 32-0694, top), Nb_2O_5 (JCPDS No. 7-0061, middle) and NiO (JCPDS No. 4-0835, bottom).

College of Chemistry and Chemical Engineering, Inner Mongolia University, Hohhot, Inner Mongolia 010021, P. R. China.
E-mail: wang_xiao_jing@hotmail.com; Fax: +86-471-4992981; Tel: +86-471-4344579

† Electronic supplementary information (ESI) available: Experimental details, XRD, comparison data, UV-vis absorption spectra. See DOI: 10.1039/c3cc49825e

similar ionic radii of Ni^{2+} (0.069 nm) and Nb^{5+} (0.064 nm), the mutual substitution between the two cations is possible[8] which gives rise to abundant defective centers due to the charge compensation effect, resulting in structural symmetry breakdown and highly disordered feature. Dislocation of cations and high density defects in the rigid framework will lead to short-ordered atomic configurations that may produce anisotropic strain gradients and the subsequent diffraction peak broadening.[9] High temperature calcination of $NiNb_2O_6$ NPs confirmed the formation of a $NiNb_2O_6$ structure (ESI-2†). The average crystallite size calculated from the broadening of the (062) plane using Scherrer's formula was ~27 nm (ESI-3†). To characterize the structural and defective feature, transmission electron spectroscopy (TEM) and high resolution TEM (HRTEM) were performed. The as-prepared $NiNb_2O_6$ NPs exhibited irregular shapes with a diameter less than 100 nm (Fig. 1b), which is larger than XRD calculated results. From a single particle, the spacing between adjacent lattice fringes was 0.252 nm (Fig. 1c), which is close to that of 0.251 nm for the (002) plane of $NiNb_2O_6$, indicating the crystalline nature of $NiNb_2O_6$ NPs. On the basis of the fast Fourier transform (FFT) analysis of the lattice fringes (inset of Fig. 1c and ESI-4†), it is seen that the $NiNb_2O_6$ NPs are surrounded with facets parallel to the terminated (002), (032), (062) and (060) edges. In addition, the atomic ratio of Ni/Nb determined by EDS was about 0.485. EDS maps of $NiNb_2O_6$ nanocrystals indicated that all detected signals dispersed homogeneously (ESI-5†). All these results confirmed the formation of *Columbite*-type $NiNb_2O_6$ NPs. Fig. 1d shows the optical diffuse reflectance spectrum of $NiNb_2O_6$ NPs. $NiNb_2O_6$ NPs exhibited a broad absorption in the range of 250–450 nm, which is attributed to a charge transfer from the oxygen ligands to the central niobium atom inside the NbO_6 group.[4] The absorption edge is at around 410 nm and the band gap energy is E_g = 3.02 eV.

Catalytic reduction of 4-NP to 4-AP with excess $NaBH_4$ has frequently been used as a model reaction to evaluate the catalytic activity of various metallic NPs.[10] Though the reaction between 4-NP and $NaBH_4$ is thermodynamically favored,[10] the reaction will not proceed in the absence of a catalyst, which can be confirmed by the absorption peak which remained unaltered with reaction time in the absence of $NiNb_2O_6$ NPs (ESI-6†). Upon the addition of $NiNb_2O_6$ NPs, the absorption peak at 400 nm gradually decreased and a peak appeared at ~305 nm with a gradual increase in intensity (Fig. 2a), indicating the transformation of 4-NP to 4-AP.[11,12] Unexpectedly, UV light irradiation can accelerate the reduction rate (Fig. 2b). The catalytic reduction efficiency of $NiNb_2O_6$ NPs was estimated to be 95.7% within 18 minutes, which was accelerated to show an apparent reduction efficiency of 94.7% within 7 minutes (Fig. 2c).

Further comparative studies indicated that the concentration changes of 4-NP with reaction time varied in terms of an exponential decay (Fig. 2c). As a result, the $\ln(C_0/C_t)$ plots show a linear relationship with reaction time either in the dark or under UV light irradiation, indicating that reduction of 4-NP proceeds through a pseudo-first-order kinetic reaction, $\ln(C_0/C_t) = k_{app}t$, where C_0 and C_t are the initial and actual concentration of the 4-NP solution at time t, respectively, and k_{app} is the apparent rate constant. The apparent

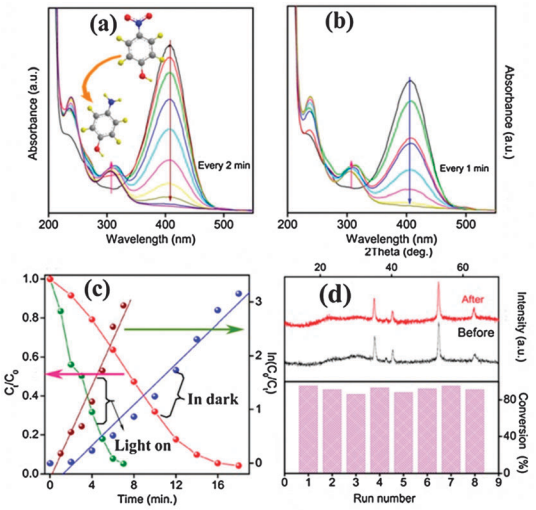

Fig. 2 UV-vis absorption spectra recorded during the catalytic reduction of 4-NP over $NiNb_2O_6$ NPs at 25 °C in the dark (a) and under UV light irradiation (b). Residual fraction of 4-NP in solution as a function of reaction time upon treatment with $NiNb_2O_6$ NPs (c). XRD patterns of $NiNb_2O_6$ NPs before and after the transformation reaction (top), and conversion efficiency of 4-NP to 4-AP when catalyzed by $NiNb_2O_6$ NPs for different runs (bottom) (d).

rate constant determined from the slope was 0.19 ± 0.02 min^{-1} for $NiNb_2O_6$ NPs in the dark. Surprisingly, the apparent rate constant of $NiNb_2O_6$ NPs was highly enlarged to 0.43 ± 0.04 min^{-1} under UV light irradiation. In order to compare our result with literature values, we calculated the ratio of the apparent rate constant k_{app} to the total mass of the catalyst ($k = k_{app}/m$). The activity factors for $NiNb_2O_6$ NPs without and with UV light irradiation were determined to be 633.3 min^{-1} g^{-1} and 1433 min^{-1} g^{-1}, respectively, which are much larger than those reported previously for several noble metal NPs (ESI-7†). Fig. 2d shows the XRD patterns of $NiNb_2O_6$ NPs before and after catalytic reaction. No structural difference between the samples before and after reaction is observable, confirming the high stability and well reducing capacity of $NiNb_2O_6$ NPs, the reducing capacity of $NiNb_2O_6$ NPs was well-preserved after eight cycles of redox reactions.

Having these results in mind, it is highly necessary to investigate the underlying photo-synergistic mechanism. To fully understand the mechanism, several factors should be taken into consideration, such as active sites, defect chemistry, electronic structures and so forth. With regard to the active sites, many investigations have demonstrated that the reduction reaction is dominated by the co-adsorption of 4-nitrophenate ions and borohydride ions, which overcomes the kinetic barrier for the reaction and initiates the electron transfer on metallic NP surfaces.[11] If Nb^{5+} ions at surfaces were the active centers, several niobate-based NPs should be active for this reaction. Three niobate-based NPs were employed to test the reactivity of Nb^{5+}, which exhibited no apparent activity (ESI-8†), suggesting that Nb^{5+} ions are likely irrelevant to the electron transfer process in the dark. According to previous literature, anions, oxygen vacancies, surface hydrogen species do not participate in the reduction of 4-NP.[13] Therefore, it is reasonable to expect that Ni^{2+} ions may

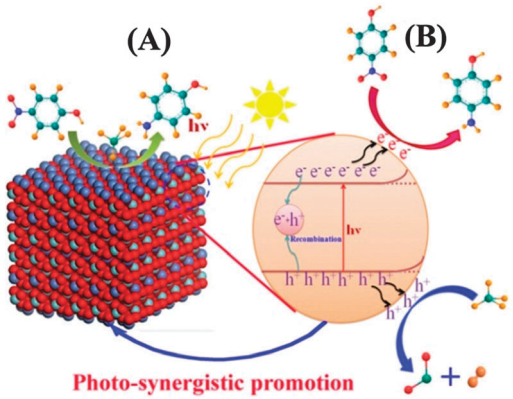

Fig. 3 Schematic illustration of the photo-synergistic catalytic reaction for the reduction 4-NP to 4-AP in an aqueous solution of $NaBH_4$ upon UV light irradiation at room temperature on a $NiNb_2O_6$ catalyst.

act as the active centers for electron transfer (Fig. 3A process) because Ni based alloys and oxides showed highly catalytic activity in the reduction of nitrobenzenes.[5,14] In addition, defect chemistry also has a critical impact on the catalytic activity of $NiNb_2O_6$ NPs. The disordered structure will give rise to a large number of defective centers, such as oxygen vacancies, surface cations *etc.* Though these defective centers are inactive to this reaction, they can promote the adsorption of reactive species and facilitate the electron transfer on NP surfaces.[6] Meanwhile, the disordered structure led to exposure of massive Ni^{2+} active sites in comparison to the calcined bulk one which can also enhance the catalytic activity (ESI-9†).

Most importantly, the electronic structure of $NiNb_2O_6$ NPs plays significant roles in the photo-synergistic reaction promoting the reduction of 4-NP, which makes $NiNb_2O_6$ act as the unique catalyst differing from the ever reported metallic or metal oxide NPs. Basically, the photocatalytic process of semiconductors involves electron–hole pairs after light irradiation, which could recombine in the bulk or migrate to the surfaces to react with adsorbed species. Therefore, the reductive capability of the photogenerated electrons is extremely dependent on the potential of the conduction band. For instance, the conduction band potential of CdS is −0.8 to −1.0 V *vs.* NHE, which is more negative than standard reduction potentials for 4-NP/4-AP.[7] The photoreduction reaction proceeds *via* electron transfer from the NP surface to the nitrogroups and leads to the reduction of 4-NP in the presence of a hole scavenger. Although the band edge positions are not easily determined experimentally, a theoretical prediction is possible using concepts of Mulliken electronegativity (ESI-10†). The apparent E_{CB} of $NiNb_2O_6$ nanocrystals is determined to be −0.62 V *vs.* NHE, which is more positive than that of 4-NP/4-AP (−0.76 V *vs.* NHE). This suggests that the photoreduction of 4-NP by $NiNb_2O_6$ NPs cannot be achieved, which can also be confirmed by the photoreduction of 4-NP using ammonium oxalate as the hole scavenger (ESI-11†). However, it is well accepted that the electronic structure of semiconductors is extremely dependent on surface structures. Typically, adsorbates undergo chemisorption on the semiconductor surfaces, giving rise to a negatively charged surface, resulting in an upward band bending.[15] For the present $NiNb_2O_6$ NPs, the adsorption of borohydride ions led to surface rearrangement of $NiNb_2O_6$ NPs and created a negatively charged surface as depicted by the variation of zeta potential from 28.6 mV to −40 mV in aqueous solution after addition of $NaBH_4$.[16] It is undoubtedly that the rearranged $NiNb_2O_6$ surfaces gave rise to an upward band bending that improved the reductive capability of photogenerated electrons and accelerated the reduction rate (Fig. 3B process). Therefore, a synergy between A and B processes leads to highly efficient catalytic performance.

In summary, a novel catalyst exhibited outstanding activity and stability toward catalytic reduction of 4-NP to 4-AP. The underlying mechanism is completely different from those previously reported for metallic NPs. This work may provide new possibilities for the development of novel catalytic systems and bring opportunities for many electron transfer reactions that need to be catalyzed.

This work was financially supported by NSFC (Grants 21103081, 21367018, 21267014).

Notes and references

1 F. Zaera, *Chem. Soc. Rev.*, 2013, **42**, 2746.
2 X. Huang, X. P. Liao and B. Shi, *Green Chem.*, 2011, **13**, 2801.
3 (*a*) J. Wang, X. B. Zhang, Z. L. Wang, L. M. Wang, W. Xing and X. Liu, *Nanoscale*, 2012, **4**, 1549; (*b*) S. Wu, J. Kaiser, X. Guo, L. Li, Y. Lu and M. Ballauff, *Ind. Eng. Chem. Res.*, 2012, **51**, 5608.
4 Y. Y. Zhou, M. K. Lü, Z. F. Qiu, A. Y. Zhang, Q. Ma, H. P. Zhang and Z. S. Yang, *Mater. Sci. Eng., B*, 2007, **140**, 128.
5 K. L. Wu, X. W. Wei, X. M. Zhou, D. H. Wu, X. W. Liu, Y. Ye and Q. Wang, *J. Phys. Chem. C*, 2011, **115**, 16268.
6 Y. G. Su, J. Y. Lang, L. P. Li, K. Guan, C. F. Du, L. M. Peng, D. Han and X. J. Wang, *J. Am. Chem. Soc.*, 2013, **135**, 11433.
7 A. Hernández-Gordillo, A. G. Romero, F. Tzompantzi, S. Oros-Ruiz and R. Gómez, *J. Photochem. Photobiol., A*, 2013, **257**, 44.
8 E. Heracleous, A. Delimitis, L. Nalbandian and A. A. Lemonidou, *Appl. Catal., A*, 2007, **325**, 220.
9 (*a*) V. Petkov, T. Ohta, Y. Hou and Y. Ren, *J. Phys. Chem. C*, 2007, **111**, 714; (*b*) R. Jothiramalingam and M. K. Wang, *J. Porous Mater.*, 2010, **17**, 677; (*c*) M. B. Kerber, M. J. Zehetbauer, E. Schafler, F. C. Spiechermann, S. Bernstorff and T. Ungar, *JOM*, 2011, **63**, 61.
10 R. Bhandari and M. R. Knecht, *ACS Catal.*, 2011, **1**, 89.
11 S. Saha, A. Pal, S. Kundu, S. Basu and T. Pal, *Langmuir*, 2010, **26**, 2885.
12 Z. Y. Zhang, C. L. Shao, Y. Y. Sun, J. B. Mu, M. Y. Zhang, P. Zhang, Z. C. Guo, P. P. Liang, C. H. Wang and Y. C. Liu, *J. Mater. Chem.*, 2012, **22**, 1387.
13 J. Su, X. Zou, G. Li, L. Li, J. Zhao and J. Chen, *Chem. Commun.*, 2012, **48**, 9032.
14 N. Bayal and P. Jeevanandam, *J. Alloys Compd.*, 2012, **537**, 232.
15 M. J. Li, G. C. Xing, L. F. N. A. Qune, G. Z. Xing, T. Wu, C. H. A. Huan, X. H. Zhang and T. C. Sum, *Phys. Chem. Chem. Phys.*, 2012, **14**, 3075.
16 S. Cho, J. Jang, J. Park, S. Jung, S. Jeong, J. Kwag, J. S. Lee and S. Kim, *J. Mater. Chem. C*, 2013, **1**, 4497.